Medical Physics
The International Journal of Medical Physics Research and Practice

Exogenous contrast agents for thermoacoustic imaging: An investigation into the underlying sources of contrast

Olumide Ogunlade and Paul Beard

Citation: Medical Physics **42**, 170 (2015); doi: 10.1118/1.4903277
View online: http://dx.doi.org/10.1118/1.4903277
View Table of Contents: http://scitation.aip.org/content/aapm/journal/medphys/42/1?ver=pdfcov
Published by the American Association of Physicists in Medicine

Exogenous contrast agents for thermoacoustic imaging: An investigation into the underlying sources of contrast

Olumide Ogunlade[a] and Paul Beard
Department of Medical Physics and Biomedical Engineering, University College London, London WC1E 6BT, United Kingdom

(Received 10 June 2014; revised 11 September 2014; accepted for publication 11 November 2014; published 22 December 2014)

Purpose: Thermoacoustic imaging at microwave excitation frequencies is limited by the low differential contrast exhibited by high water content tissues. To overcome this, exogenous thermoacoustic contrast agents based on gadolinium compounds, iron oxide, and single wall carbon nanotubes have previously been suggested and investigated. However, these previous studies did not fully characterize the electric, magnetic, and thermodynamic properties of these agents thus precluding identification of the underlying sources of contrast. To address this, measurements of the complex permittivity, complex permeability, DC conductivity, and Grüneisen parameter have been made. These measurements allowed the origins of the contrast provided by each substance to be identified.
Methods: The electric and magnetic properties of the contrast agents were characterized at 3 GHz using two rectangular waveguide cavities. The DC conductivity was measured separately using a conductivity meter. Thermoacoustic signals were then acquired and compared to those generated in water. Finally, 3D electromagnetic simulations were used to decouple the different contributions to the absorbed power density.
Results: It was found that the gadolinium compounds provided appreciable electric contrast but not originating from the gadolinium itself. The contrast was either due to dissociation of the gadolinium salt which increased ionic conductivity or its nondissociated polar fraction which increased dielectric polarization loss or a combination of both. In addition, very high concentrations were required to achieve appreciable contrast, to the extent that the Grüneisen parameter increased significantly and became a source of contrast. Iron oxide particles were found to produce low but measurable dielectric contrast due to dielectric polarization loss, but this is attributed to the coating of the particles not the iron oxide. Single wall carbon nanotubes did not provide measurable contrast of any type.
Conclusions: It is concluded that gadolinium based contrast agents, iron oxide particles, and single walled carbon nanotubes have little intrinsic merit as thermoacoustic contrast agents. Simple electrolytes such as saline which yield high contrast based on ionic conductivity provide much higher dielectric contrast per unit solute concentration and are likely to be significantly more effective as contrast agents. [http://dx.doi.org/10.1118/1.4903277]

Key words: thermoacoustic imaging, contrast agents, complex permittivity, conductivity, Gruneisen parameter

1. INTRODUCTION

Thermoacoustic imaging is a hybrid imaging modality based on the absorption, by tissue, of short pulses of electromagnetic (EM) radiation in the radio frequency or microwave part of the EM spectrum. This is in contrast to photoacoustic imaging where the EM excitation lies in the optical part of the spectrum.[1] The result of the absorption is a rapid localized pressure increase which in turn gives rise to propagating ultrasound waves. If these ultrasound waves are recorded at multiple spatial locations over the tissue surface, an image of the initial pressure distribution (p_0) due to EM absorption can be reconstructed. Assuming the thermal and stress confinement conditions are satisfied, the initial pressure distribution at a spatial location r as a result of the absorbed EM energy density $H(r)$ can be written as

$$p_0(r) = \Gamma H(r), \tag{1}$$

where Γ is known as the Grüneisen parameter, a dimensionless thermodynamic constant that gives an indication of how efficiently the absorbed energy is converted to pressure.

The absorbed energy can be considered in terms of absorbed power. The power deposited in a volume of tissue depends on the electric and magnetic properties of the tissue, and is given by Poynting's relation of energy conservation[2,3]

$$\Re\left(\oint_S \mathbf{E}\times\mathbf{H}^*\cdot d\mathbf{s}\right) = -\omega\int_V(\mu_0\mu_r''\mathbf{H}\cdot\mathbf{H}^* + \epsilon_0\epsilon_r''\mathbf{E}\cdot\mathbf{E}^*)dv - \int_V(\sigma_c\mathbf{E}\cdot\mathbf{E}^*)dv, \tag{2}$$

where the volume V of tissue is characterized by the complex permittivity ($\epsilon = \epsilon_0[\epsilon_r' - j\epsilon_r'']$), complex permeability ($\mu = \mu_0[\mu_r' - j\mu_r'']$), and ionic conductivity (σ_c). The subscript 0 represents the free space values of the parameter, while subscript r represents the values of the parameter relative to

free space. **E** and **H** represent the electric field intensity (V/m) and magnetic field intensity (A/m), respectively, inside the volume. The left hand side of Eq. (2) represents the net real electromagnetic power transmitted across the closed surface S containing volume V. The first, second, and third terms on the right hand side of Eq. (2) represent the power deposited inside the tissue volume due to magnetic loss, dielectric polarization loss, and joule heating, respectively. The dielectric polarization loss term $\omega\epsilon_0\epsilon_r''$ can be replaced by an equivalent conductivity σ_d. The power deposited per unit volume is then given by

$$P_d = \omega\mu_0\mu_r''\mathbf{H}\cdot\mathbf{H}^* + (\sigma_d + \sigma_c)\mathbf{E}\cdot\mathbf{E}^*. \quad (3)$$

At microwave frequencies,[4] the water content of tissue dominates the dielectric polarization loss term σ_d in Eq. (3). This term is a frictional damping loss that arises from the time-varying reorientation of permanent dipoles of water molecules in the presence of an applied electric field, and is frequency dependent. The ionic content of tissue determines σ_c and is generally frequency independent.[5] In tissue, μ_r'' is negligible at microwave frequencies, so the first term on the right hand side of Eq. (3) can be omitted. Hence, in thermoacoustic imaging, the endogenous contrast results from the total conductivity $\sigma_t = \sigma_d + \sigma_c$.[6,7] In general, imaging modalities based on microwave interactions lack the spectroscopic selectivity of optical based techniques. This is because the σ_t spectrum of tissue is dominated by the σ_d spectrum of water which, at microwave frequencies, is relatively featureless and described by a single Debye relaxation.[8] Thermoacoustic imaging also lacks the strong differential contrast found in photoacoustic imaging, due to the small differences in σ_t between different high water content tissues. This leaves the difference in σ_t between high water content tissue and adipose dominated tissue as the principal source of exploitable endogenous contrast.[9,10] As a consequence, there is a need for exogenous contrast agents, in order to improve the differential contrast for high water content tissue and increase the signal to noise ratio.

Exogenous contrast agents, such as iron oxide particles,[11,12] carbon nanotubes,[13,14] carbon nanoparticles,[15] and Magnevist®[16] (a gadolinium based contrast agent used in magnetic resonance imaging), have been investigated for use in thermoacoustic imaging. In these previous studies, the contrast agents were assessed by comparing the thermoacoustic signal amplitude generated by the contrast agent relative to that of water. However, independent measurements of the complex permittivity, complex permeability, or ionic conductivity were not undertaken except in Ref. 11, where only the complex permittivity of solutions of iron oxide particles was measured. As Eqs. (1) and (2) indicate, all of these parameters contribute to the absorbed power and thus the thermoacoustic signal amplitude. Hence, these previous studies did not reveal the underlying source of contrast provided by these agents.

This paper seeks to address the above issues by first describing measurements of the electric and magnetic properties at 3 GHz (Ref. 17) of various contrast agents including three gadolinium based contrast agents, iron oxide particles, single walled carbon nanotubes, sodium chloride (NaCl), and sucrose, before describing the generation of thermoacoustic signals and determining the Grüneisen parameter of the contrast agents. The paper is structured as follows: Sec. 2 describes the cavity resonator method used to characterize the electric and magnetic properties of the contrast agents in Sec. 2.A. The details of the single point thermoacoustic measurements setup is given in Sec. 2.B, and the absorbed power density simulations in Sec. 2.C. In Sec. 3, the results of the EM characterization of the contrast agents is given in Sec. 3.A and the thermoacoustic measurements are presented in Sec. 3.B., followed by a discussion of the various contributions to the thermoacoustic contrast.

2. METHODS

2.A. Complex permittivity and permeability measurements

A resonant cavity perturbation technique was used to characterize the electric and magnetic properties of the contrast agents at 3 GHz. This offers high sensitivity for single frequency measurements of both complex permeability and permittivity, compared to other techniques[18,19] such as the coaxial probe method.[11] The coaxial probe also has the disadvantage of being unable to measure the magnetic properties of the contrast agent.

To form the resonant cavity, the ends of a rectangular waveguide were closed with metal blocks. A standing wave is set up inside the cavity when energy is coupled into it through coaxial connectors attached to the cavity. The inner conductors of the coaxial connectors protrude slightly into cavity. The coaxial connectors are connected to a vector network analyzer (Rohde Schwarz FSH8), which measures the transmission coefficient between the two coaxial ports. The resonant frequency and Q-factor (ratio of resonant frequency to the 3 dB bandwidth) can then be determined from the measured transmission coefficient. Since the network analyzer measures discrete frequency points, the Lorentzian quadratic curve fitting method[20] is used to improve the accuracy of the measurements. Two rectangular cavities were used, a custom designed rectangular waveguide [shown in Fig. 1(a)][21] and a standard S band (WR-284) waveguide. The resonant modes of the two cavities are TE_{101} and TE_{102} modes, respectively. The dimensions, resonant frequency (f_0), and Q-factor (Q_0) of the cavities without the sample, are presented in Table I.

The insertion of an absorber into a cavity causes perturbation of the cavity fields. This produces a change in the measured transmission coefficient and thus the resonant frequency and Q-factor of the cavity. Figure 1(b) shows an example of the transmission coefficient measured for the TE_{101} mode cavity perturbed by saline solutions of different concentrations. These changes are then used to obtain the dielectric properties of the absorber, using the expressions given below Eq. (4).[19,22] An essential condition for the use of Eq. (4) is that the ratio of EM energy stored in the absorber to the EM energy stored in the cavity is small, so that the Q-factor of the perturbed cavity remains sufficiently large[23,24]

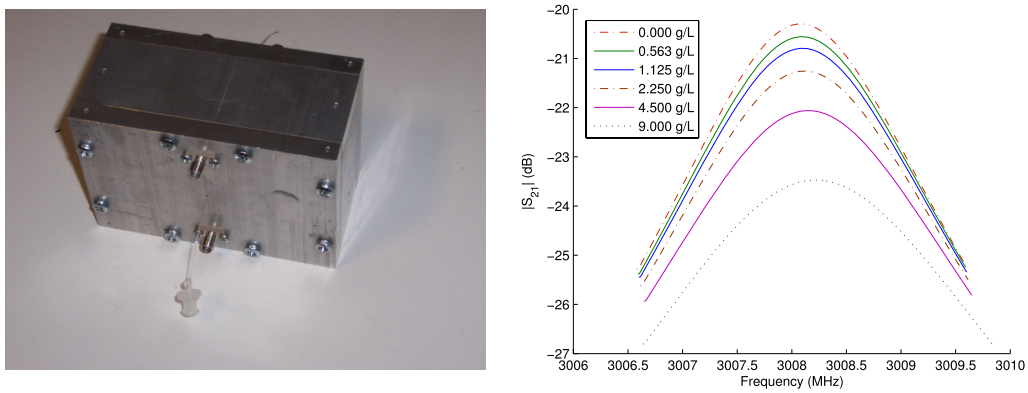

FIG. 1. (a) The TE_{101} mode cavity. (b) Measured transmission coefficient of the TE_{101} mode cavity containing saline solutions. (c) |E| distribution in the TE_{101} mode cavity showing maximum |E| field at the center where the absorber is located. (d) |H| distribution in the TE_{101} mode cavity showing minimum |H| field at the center where absorber is located.

$$\epsilon_r' = \left(\frac{f_0 - f}{f_0}\right)\frac{V_c}{2V_s} + 1,$$
$$\sigma_t = \omega\epsilon_0\left(\frac{1}{Q} - \frac{1}{Q_0}\right)\frac{V_c}{4V_s},$$
$$\mu_r' = \left(\frac{d^2 + 4a^2}{8a^2}\right)\left(\frac{f_0 - f}{f_0}\right)\frac{V_c}{V_s} + 1,$$
$$\mu_r'' = \left(\frac{d^2 + 4a^2}{16a^2}\right)\left(\frac{1}{Q} - \frac{1}{Q_0}\right)\frac{V_c}{V_s}. \quad (4)$$

V_c and V_s represent the volumes of the cavity and absorber, respectively, while f and Q are the resonant frequency and Q-factor of the cavity, respectively, after perturbation. All other variables are as given in Table I. The absorber is contained inside a low loss polymer tube with inner diameter of 250 μm and outer diameter 500 μm. For measuring the complex permittivity, the absorber is inserted in the center of the TE_{101} mode cavity, where the electric field is maximum (magnetic field minima). The absorber is oriented parallel to the electric field inside the cavity. For measuring the magnetic properties, the absorber is oriented parallel to the magnetic field and is inserted at a location in the TE_{102} mode cavity where the magnetic field has a maxima (electric field minima).

The electric loss term (σ_t) estimated using Eq. (4) represents the total electric loss in the absorber at 3 GHz. Therefore, in order to determine the contribution of σ_c, the DC conductivity was measured separately using a conductivity meter (HI 99300, Hannah instruments). The dielectric polarization loss contribution is then given by $\sigma_d = \sigma_t - \sigma_c$.

2.B. Thermoacoustic signal measurement

A schematic of the experimental arrangement used to acquire thermoacoustic signals is shown in Fig. 2. The excitation source is a pulsed microwave source with a carrier frequency of 3 GHz. The peak power of the source was 30 KW and pulse width was 250 ns. The pulse repetition frequency was 1300 Hz. The microwave power was delivered to the absorber using a rectangular waveguide antenna with inner cross section dimensions of 72.2 mm (width) by 34.4 mm

TABLE I. Dimensions, resonant frequency, and Q-factor of waveguide cavities.

Resonant mode	Width a (mm)	Height b (mm)	Length d (mm)	f_0 (GHz)	Q_0
TE_{101}	95	38	58	3.012	4967
TE_{102}	72.2	34.2	135.6	3.047	6045

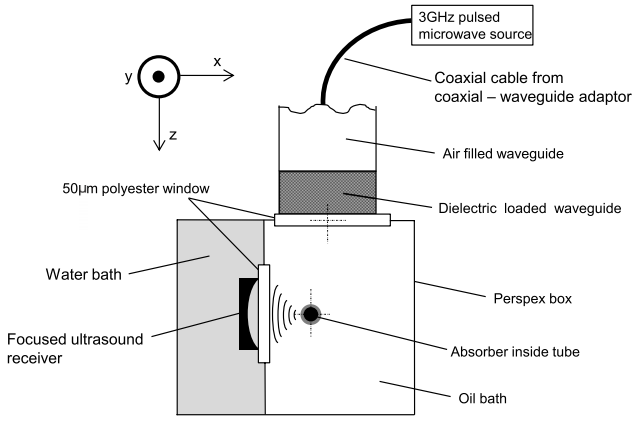

FIG. 2. Schematic of experimental arrangement used to acquire thermoacoustic signals.

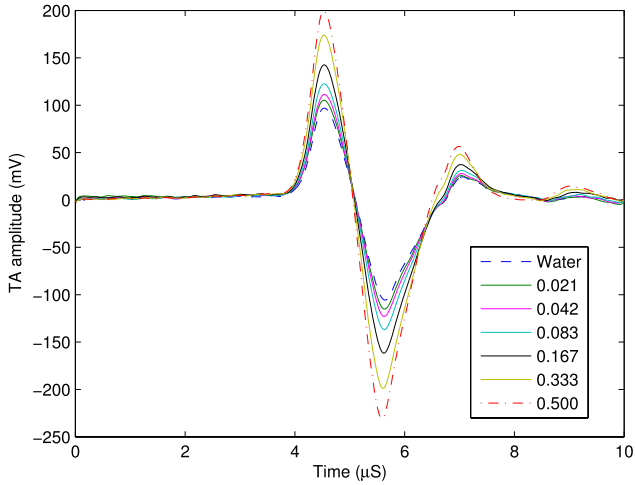

FIG. 3. Single point thermoacoustic signals generated in Magnevist solutions with volume fraction in deionized water, increasing in ascending order from 0 (dashed line) to 0.5 (dashed–dotted line).

(height). A section of the antenna was loaded with a piece of Teflon, a quarter wavelength long, to match the impedance of the antenna to the wave impedance in sunflower oil, into which the absorber was placed. The absorber was placed in oil because oil is lossless to microwave propagation while providing the necessary acoustic coupling. The EM field radiated from the antenna is linearly polarized in the y–z plane of Fig. 2.

The absorber is contained in a flexible polymer tube with an inner diameter of 2 mm and an outer diameter of 2.8 mm and was placed at a fixed position 20 mm from the antenna (within the antenna near field), with its axis parallel to the antenna's linear polarization plane. The absorber can be regarded as an electrically thin cylinder because the excitation wavelength (10 cm) is much larger than the tube diameter (d) of 2 mm. For such a geometry, where $d \ll \lambda$, $|E|$ inside the tube increases when d increases.[25] This results in an increase in P_d, and thus the TA signal amplitude. However, as d increases, the frequency content of the TA signal from a uniformly illuminated tube also reduces, becoming lower than the central frequency of the transducer bandwidth, where the sensitivity is the highest. The tube diameter of 2 mm was chosen on the basis that it represented the optimum compromise between these two factors. The absorber was offset relative to the center of the waveguide by approximately 10 mm. One reason for this was to ensure that the absorber was located at roughly the focal distance (32 mm) of the ultrasound transducer. Another reason was to minimize the reflection coefficient seen by the source, due to the loading effects of an absorber placed in the near field of the matched antenna. The loading effects of the absorber are greatest along the central axis of the waveguide, where the radiated electric field is maximum.

A 3.5 MHz cylindrically focused ultrasound transducer (Panametrics V383) was placed in deionized water to receive the generated ultrasound signals. The transducer was chosen to match the geometry of the absorber and was oriented with its focusing plane normal to the axis of the tube. The deionized water was contained in the same tank as the oil, the two separated by a 50 μm polyester film window, which is assumed to be acoustically transparent. The transducer output was amplified by a 8 dB preamplifier (Precision Acoustics), and further by a 60 dB amplifier (Analog modules 322-8-B). The thermoacoustic signals were acquired using a data acquisition card (NI PCI 5112 sampled at 100 MS/s, with an analog bandwidth of 50 MHz), and were averaged over 100 pulses. As a postprocessing step in MATLAB, the recorded thermoacoustic signal was passed through a low pass filter with a bandwidth of 10 MHz, before extracting the peak-to-peak value. A filter bandwidth of 10 MHz is reasonable, because the −6 dB bandwidth of the ultrasound transducer is from 1.68 to 4.64 MHz (93.83% fractional bandwidth at a center frequency of 3.16 MHz). An example of the thermoacoustic signals for varying volume fractions of a solution of Magnevist in water is shown in Fig. 3, with the worst case SNR of 29.2 dB for deionized water.

2.C. Electromagnetic simulation

In order to identify the sources of contrast, there is a need to simulate the experimental arrangement in Sec. 2.B. The simulation is required to decouple the various contributions to the absorbed power density P_d. A cursory glance at Eq. (3) may suggest P_d is a simple function of σ_t and μ_r''. However, P_d also depends on $\mathbf{E}$ and $\mathbf{H}$, which themselves are functions of ϵ_r', σ_t, μ_r', and μ_r''. Additionally, $\mathbf{E}$ and $\mathbf{H}$ also depend on the absorber geometry, the location of the source relative to the absorber (near or far field), as well as the polarization of the incident wave.[26,27]

In this work, CST®, a commercial 3D full wave EM solver was used to simulate the P_d distribution. The solver which is based on the finite element method, uses an adaptive tetrahedral mesh. The P_d distribution for the geometry described in Sec. 2.B was simulated using the values of the electric and magnetic properties measured for each contrast agent as described in Sec. 2.A. A single value of P_d, which is proportional to the TA signal amplitude, is then obtained by integrating the simulated P_d distribution over the cross section of

the tube. This is valid because the ultrasound transducer used in the TA experiments is cylindrically focused onto a plane.

3. RESULTS AND DISCUSSION

3.A. Characterization of electric and magnetic properties

The complex permittivity and permeability of four contrast agents were measured using the two resonant cavities described in Sec. 2.A. The first three are paramagnetic gadolinium based contrast agents: Magnevist®, Dotarem®, and Prohance®, which are supplied off-the-shelf in concentrations of 0.5 M. Magnevist has previously been investigated as a TA contrast agent.[16] For comparison, Dotarem and Prohance both of which contain different gadolinium compounds to Magnevist, were also characterized in the current study. The fourth contrast agent was a superparamagnetic carboxydextran coated iron oxide based contrast agent, EM1301 (Endomagnetics Ltd., United Kingdom) containing 0.5 M of iron as iron oxide nanoparticles. All four contrast agents are approved for clinical use. The gadolinium based contrast agents are used in clinical MRI, while EMC1301 is approved for use as a magnetic tracer in sentinel lymph node detection. In addition, the complex permittivity of water, NaCl solution, and sucrose (Sigma Aldrich S8501) solution was also measured. NaCl and sucrose were characterized as reference absorbers because their chemical behavior in solution is well understood. The concentration of sucrose was 0.5 M, while the saline solution contained 0.154 M (9 g/L) NaCl, as used in intravenous infusions. All measurements were conducted at a room temperature of 21 °C and are presented in Table II.[28] The measured values of ϵ_r' and σ_t of water agree well with values of 77.96 and 2.131, respectively, reported previously in Ref. 29 at 20 °C.

3.A.1. Electric properties of saline and sucrose solutions

As noted in Sec. 1, σ_t is made up of the dielectric polarization loss term σ_d and the ionic conductivity loss term σ_c. In order to illustrate the two loss contributions separately, the dielectric properties of sodium chloride and sucrose were measured. Sodium chloride is an electrolyte which provides only σ_c contrast, while sucrose is a polar nonelectrolyte and therefore provides only σ_d contrast. When NaCl is introduced into water, it dissociates into mobile Na^+ and Cl^- ions. It is the presence of these mobile ions, that gives rise to an increase in σ_c, and thus σ_t. This is as shown in Table II where σ_c of the saline is 1.41 S/m, compared to 0.0002 S/m for water. NaCl is termed a strong electrolyte because it wholly dissociates in solution into ions of Na^+ and Cl^-. Sucrose, on the other hand, is not an electrolyte because when sucrose molecules undergoes solvation, they remain intact as aqueous sucrose molecules and do not release any ions into the solution. The small increase in σ_c of the sucrose solution in Table II (0.0021 S/m compared to 0.0002 S/m for water) is most likely due to the presence of small impurities in the solute (99.5% purity). The presence of impurities does not however explain the significant increase in σ_t of the sucrose solution. This increase is due to an increase in σ_d which arises from the dielectric polarization loss of the sucrose molecules and the dielectric polarization loss of the hydration sheath around the sucrose molecules.[30]

The dielectric properties of different concentrations of saline are given in Table III. As expected, σ_c increases with increasing NaCl concentration. The small reduction in σ_d, with increase in the solute concentration, is due to a reduction in the number of polar water molecules per unit volume that are free to rotate. For the sucrose solutions in Table IV, σ_t is almost solely due to σ_d, since σ_c is negligible for all concentrations. For both the saline and sucrose solution in Tables III and IV, a decrease in ϵ_r' (dipole moment per unit volume) is observed, as the solute concentration increases. This is because as the solute concentration increases, more water molecules are displaced in the volume by the solute.[31] The effective dipole moment per unit volume of the solution therefore decreases, because water has a large dipole moment relative to its volume (hence high value of ϵ_r'), compared to most substances.

3.A.2. Electric properties of gadolinium based contrast agent solutions

The relatively large values of the ionic conductivity (σ_c) of the 0.5 M solutions of Magnevist and Dotarem in Table II suggest that Magnevist and Dotarem are electrolytic solutions. By contrast, Prohance has a much smaller value of σ_c, suggesting it is not an electrolytic solution. The electrolytic behavior of Magnevist and Dotarem arises, because both contain gadolinium chelates which are anionic, unlike the gadolinium chelate in Prohance which is neutral.[32,33] Note that Table II shows that

TABLE II. Complex permittivity and complex permeability of 0.5 M contrast agents.

Contrast agent	ϵ_r'	$\sigma_t\|_{3\ \mathrm{GHz}}$ (S/m)	σ_c (S/m)	$\sigma_d\|_{3\ \mathrm{GHz}}$ (S/m)	μ_r'	$\mu_r''\times10^{-2}$
Magnevist (Gd based)	49.75	3.320	0.568	2.752	1.474	0.88
Dotarem (Gd based)	56.65	3.402	0.435	2.967	1.276	0.29
Prohance (Gd based)	60.54	2.857	0.0504	2.807	1.690	2.00
EM1301 (Fe based)	74.70	2.281	0.0097	2.271	1.886	4.40
Sucrose	71.93	2.487	0.0021	2.485	[a]	[a]
Saline[b]	75.25	3.456	1.4100	2.046	[a]	[a]
Water	77.76	2.098	0.0002	2.098	1.087	−0.01

[a]No measurements available.
[b]Physiological saline containing 0.154 M of NaCl.

TABLE III. Dielectric properties of saline solutions.

Conc. (g/L)	ϵ_r'	$\sigma_t\|_{3\ \mathrm{GHz}}$ (S/m)	σ_c (S/m)	$\sigma_d\|_{3\ \mathrm{GHz}}$ (S/m)	$\sigma_d - \sigma_{d\mathrm{water}}$ (S/m)
0.563	77.53	2.233	0.1095	2.124	0.026
1.125	77.43	2.316	0.2110	2.105	0.007
2.250	77.12	2.488	0.4070	2.081	−0.017
4.500	76.49	2.810	0.7620	2.048	−0.050
9.000	75.25	3.456	1.4100	2.046	−0.052

σ_c of the 0.5 M solution of Magnevist is less than that of the 0.25 and 0.167 M solutions in Table V. This is typical of weak electrolytes in which an initial increase in σ_c may occur as the solution is diluted. This counter-intuitive result occurs due to an initial increase in the dissociation of the solute into ions, with dilution.[34] Once the dissociation is complete, σ_c reduces with further dilution of the solution as expected.

The molar ionic conductivities of 0.5 M solutions of compounds containing the same gadolinium chelates as those in Magnevist, Dotarem, and Prohance, are given in Ref. 32. The calculated σ_c based on these molar ionic conductivities[35] are 5.8, 2.7, and 0.050 S/m, respectively, compared to σ_c in Table II which are 0.568, 0.435, and 0.0504 S/m, respectively. The order of magnitude smaller measured σ_c for Magnevist and Dotarem, arises from the difference in the chemical compounds characterized in Ref. 32, and those characterized in this work. In Ref. 32, sodium salts of Gd-DTPA (gadolium chelate found in Magnevist) and Gd-DOTA (gadolium chelate found in Dotarem) were characterized, whereas Magnevist and Dotarem, characterized in the current study, contain meglumine (NMG) salts of the same chelates. When the sodium salts in Ref. 32 dissociate in solution, Na^+ ions and the ions of the gadolinium chelate are released, whereas when Magnevist and Dotarem dissociate, NMG^+ ions and the ions of the gadolinium chelate are released.[36] It is the differences in size and mobility between Na^+ ions and NMG^+ ions that give rise to the differences in σ_c, with the smaller and more mobile Na^+ resulting in higher σ_c. By contrast, σ_c of 0.0504 S/m measured for Prohance in this work, agrees well with 0.050 S/m calculated from Ref. 32. This is because the chemical compound characterized in Ref. 32 is the same as the one contained in Prohance. The gadolinium chelate in Prohance (Gd-[HP-D03A]) does not require a salt of meglumine or sodium, hence it does not dissociate in solution, thus its σ_c is low. In Ref. 16, one of the reasons for suggesting Magnevist would be an effective thermoacoustic contrast agent was the assumption that it had the same high value of molar conductivity as the compound measured in Ref. 32. As mentioned above, this assumption is wrong because σ_c of Magnevist is much lower than the compound characterized in Ref. 32. In addition, the molar conductivity reported in Ref. 32 only refers to σ_c, and so does not include the contrast due to σ_d. All three gadolinium contrast agents show σ_d contrast, suggesting that they contain polar solute molecules. In the case of Magnevist and Dotarem, the polar molecules are the undissociated fraction of the weak electrolytes they contain, while in the case of Prohance which does not dissociate, it is the entire gadolium chelate.

3.A.3. Electric properties of iron oxide particles and single wall carbon nanotube solutions

From Table II, the 0.5 M solution of iron oxide particles (EM1301) has $\sigma_t = 2.281$ S/m, compared to $\sigma_t = 2.098$ S/m for water. The solution has negligible σ_c, suggesting that the particles are nonionic in solution. The increase in σ_t is due to σ_d. The increase in σ_d, and therefore the contrast provided by the EM1301 solution, is most likely due to the polar carboxydextran coating on the particles because iron oxide particles are nonpolar.

The complex permittivity (data not shown in Table II) of 1.117 mg/ml (calculated concentration ≈3.3 μM) HiPco single wall carbon nanotubes (Nanointegris Ltd) in water, with phospholipid PL-PEG-NH_2 as a dispersant, was also measured. The measured ϵ_r' was 78.78, while σ_t was 2.092 S/m at 3 GHz, and thus similar to that of water ($\epsilon_r' = 77.76$, $\sigma_t = 2.098$). This is because SWCNTs, which can be either be metallic or low conducting tubes, are nonpolar and nonionic, so provide no intrinsic contrast over water, especially at such small concentrations. These measurements support the findings of Ref. 14, in which no thermoacoustic signal was observed in solutions of SWCNT at 108 MHz (for TA contrast at 108 MHz, σ_c of SWCNTs would have to be non-negligible since $\sigma_d \approx 0$), and at 2.45 GHz found no significant heating enhancement compared to deionized water (for heating enhancement at 2.45 GHz, σ_d of SWCNTs must be greater than σ_d of water). These results contradict those reported in Ref. 13, where a twofold thermoacoustic signal enhancement was reported for a 1 mg/ml SWCNT solution, compared to water. It is unlikely that the contrast reported in Ref. 13 is due to the surfactant, since the SWCNTs in both Refs. 13 and 14 were dispersed in similar

TABLE IV. Dielectric properties of sucrose solutions.

Conc. (g/L)	ϵ_r'	$\sigma_t\|_{3\ \mathrm{GHz}}$ (S/m)	σ_c (S/m)	$\sigma_d\|_{3\ \mathrm{GHz}}$ (S/m)	$\sigma_d - \sigma_{d\mathrm{water}}$ (S/m)
85.57	74.92	2.296	0.0012	2.295	0.197
171.15	71.93	2.487	0.0021	2.485	0.387
342.30	65.59	2.836	0.0017	2.834	0.736

TABLE V. Dielectric properties of Magnevist dilutions.

Molar conc.	ϵ_r'	$\sigma_t\|_{3\ \mathrm{GHz}}$ (S/m)	σ_c (S/m)	$\sigma_d\|_{3\ \mathrm{GHz}}$ (S/m)	$\sigma_d - \sigma_{d\,\mathrm{water}}$ (S/m)
0.010	76.14	2.174	0.099	2.075	−0.023
0.021	75.45	2.282	0.169	2.113	0.015
0.042	74.04	2.476	0.286	2.190	0.092
0.083	71.41	2.764	0.442	2.322	0.224
0.167	68.00	3.034	0.626	2.408	0.310
0.250	64.46	3.296	0.702	2.594	0.496

surfactants. One possibility is the presence of an unspecified coating on the SWCNTs in Ref. 13 which could have provided the contrast. In a different study on carbon nanoparticles,[15] the reported TA contrast may be explained by the fact that the particles were synthesized out of sugar, which is known to be polar.

3.A.4. Magnetic loss

It was suggested in Ref. 16 that a measured increase in the thermoacoustic signal amplitude of a solution of Magnevist in water, compared to deionized water, could be due to losses associated with the magnetic dipole moment of the contrast agent, which would manifest as an increase in μ_r''. This is unlikely because at microwave frequencies, electric properties (ϵ_r' and σ_t) are in general several orders of magnitude greater than magnetic properties (μ_r' and μ_r'')[37] as evidenced by the data in Table II. The low magnetic loss, relative to electric loss, in Table II is unsurprising because most magnetic loss mechanisms (Hysteresis, Neil relaxation, Brownian relaxation) are low frequency (in the order of kHz–MHz) processes.[38–40] As a result, the electric loss contribution on the right hand side of Eq. (3) may be expected to be much greater than the magnetic loss at microwave frequencies.

To quantify the magnetic loss contribution to the total absorbed power density in the absorber geometry considered in this work, simulations of the absorbed power density of the gadolinium contrast agents and iron oxide particles, which are known to be magnetic, were conducted. The geometry used was that shown in Fig. 2, with the measured complex permittivity and permeability values of the contrast agents as given in Table II. The results, in Table VI, show that P_d due to magnetic loss is approximately 2 orders of magnitude smaller than P_d due to electric loss, at 3 GHz.

3.B. Thermoacoustic measurements

As described in Sec. 1, it is not sufficient to rely on the differences in total conductivity between solutions of contrast agents and water, to predict the thermoacoustic signal contrast. This is because the thermoacoustic signal also depends on ϵ_r', which influences the field distribution $\mathbf{E}$ inside the absorber, and the Grüneisen parameter Γ. For this reason, thermoacoustic experiments were undertaken to examine how the increases in total conductivity translate to changes in thermoacoustic signal amplitude.

Using the experimental setup described in Sec. 2.B, single point thermoacoustic signals were acquired for different concentrations of Magnevist, Dotarem, Prohance, saline, and sucrose solutions whose dielectric properties are detailed in Tables III–V, VII and VIII. In Fig. 4, the pk–pk thermoacoustic signal amplitude generated, for solutions of different concentrations (diluted down from one original concentration), is plotted against the total conductivity. The error bars represent the standard deviation of five different measurements on the same sample. The figure shows an increase in the thermoacoustic signal amplitude with conductivity as expected. However, if the thermoacoustic signal amplitude was simply a function of σ_t, all data points, irrespective of the contrast agent, would lie on the same curve. However, Fig. 4 shows that this is not the case. For example, the TA signal amplitude for the same value of σ_t for sucrose and saline is significantly different. As mentioned above, this could be due to changes in ϵ_r' or Γ. The influence of both of these parameters is therefore discussed in Secs. 3.B.1 and 3.B.2.

In addition (not shown in Fig. 4), the thermoacoustic signal amplitude of a 0.5 M solution of EM1301 iron oxide particles (containing 28 mg/ml of iron) was also measured. The thermoacoustic signal amplitude was approximately 1.1 times that of water. This agrees with a value of 1.09 obtained from a ratio of σ_t of EM1301 to that of water in Table II. However, this does not corroborate the reported threefold increase in TA signal amplitude for 0.2 mg/ml of iron oxide particles reported in Ref. 12, or a twofold increase for an unspecified concentration of iron oxide particles reported in Ref. 11. Any increase in TA contrast measured in Refs. 11 and 12 could not be due to the iron oxide particles themselves, because they are not polar and are nonionic. It is hypothesized that the contrast

TABLE VI. Contributions of electric loss and magnetic loss to the total absorbed power density of contrast agents.

Contrast agent	Total P_d (W/m^2)	Electric P_d (W/m^2)	Magnetic P_d (W/m^2)
Magnevist	0.5916	0.5910	0.0006
Dotarem	0.6215	0.6211	0.0003
Prohance	0.5560	0.5542	0.0018
EM1301	0.5159	0.5103	0.0056

TABLE VII. Dielectric properties of Prohance dilutions.

Molar conc.	ϵ_r'	$\sigma_t\|_{3\ \mathrm{GHz}}$ (S/m)	σ_c (S/m)	$\sigma_d\|_{3\ \mathrm{GHz}}$ (S/m)	$\sigma_d - \sigma_{d\mathrm{water}}$ (S/m)
0.010	76.35	2.117	0.003	2.114	0.016
0.021	75.99	2.144	0.005	2.139	0.041
0.042	75.35	2.201	0.009	2.192	0.094
0.083	73.95	2.304	0.017	2.287	0.189
0.167	71.17	2.471	0.030	2.441	0.343
0.250	69.64	2.550	0.041	2.509	0.411

could have resulted from either the coating on the iron oxide particles or the surfactant used to form s table suspensions of the particles, namely, citrate in Ref. 11 and a sodium salt in Ref. 12, both of which are electrolytes.

3.B.1. Effect of changes in permittivity

The thermoacoustic experimental setup in Sec. 2.B comprises a single absorber in a homogeneous, nonabsorbing background. As shown in Tables III–V, VII and VIII, an increase in σ_t of a contrast agent solution, relative to water, occurs with increase in concentration. However, this increase in σ_t with concentration is also accompanied by a reduction in the value of ϵ_r', due to the displacement of water molecules as discussed in Sec. 3.A.1. A reduction in ϵ_r' of the absorber reduces the localized electric field within the absorber, and thus P_d. Hence, to explore the effect of changes in ϵ_r', P_d was simulated for the values of ϵ_r' and σ_t given in Tables III–V, VII and VIII. The results are shown in Fig. 5, normalized to that of water, as a function of σ_t. Also shown is the simulated normalized P_d of a hypothetical contrast agent which has a fixed value of ϵ_r' set to that of water (77.76), and is independent of changes in σ_t.

For the saline solutions in Fig. 5, ϵ_r' reduces from 77.56 to 75.25 for the range of σ_t plotted, while for sucrose solutions, it reduces from 74.92 to 65.59. For a given σ_t, P_d is greater in saline, due to its higher ϵ_r'. The deviation of the curve representing the saline solutions from the hypothetical absorber is much smaller than that of the sucrose solutions. This is because the concentration of solute contained in the saline solutions (Table III) is 2 orders of magnitude smaller than sucrose (Table IV), resulting in ϵ_r' of saline remaining relatively unchanged with increase in σ_t.

As the thermoacoustic signal amplitude is proportional to P_d, the curves of the thermoacoustic signal amplitude in Fig. 4, and P_d in Fig. 5 should follow the same trends. This does not appear to be the case. For example, Fig. 5 shows that for a given σ_t, the saline solution gives a greater P_d than the sucrose solution. However, the opposite is the case in Fig. 4, where for a given σ_t, sucrose solution gives a greater thermoacoustic signal amplitude than saline. This suggests the Grüneisen parameters of the contrast agent solutions could be different, as discussed in Sec. 3.B.2.

3.B.2. Effect of changes in Grüneisen parameter

The increase in TA signal amplitude with increase in concentration of the contrast agent is usually considered to be due to the changes in the dielectric properties (ϵ_r' and σ_t). However, as the concentration of the solute increases, the thermodynamic properties of the solution, and thus its Grüneisen parameter, may also change. This change in the Grüneisen parameter will also influence the measured TA signal amplitude.[41] To investigate this, the ratio of the measured peak–peak TA signal amplitude ($\mathrm{TA}_{\mathrm{meas}}$) to the simulated P_d of the contrast agents is calculated. This ratio is proportional to the Grüneisen parameter of the solution (Γ_{sol}), scaled by a numerical constant which is a function of the measurement setup

$$\frac{\mathrm{TA}_{\mathrm{meas}}}{P_d} = K\Gamma_{\mathrm{sol}}. \tag{5}$$

Therefore, by dividing Eq. (5) for a solution of a contrast agent, by the equivalent expression for water, the constant term (K) is eliminated, and the ratio of the Grüneisen parameter of the contrast agent solution to that of water is obtained. This is shown in Fig. 6 for the solutions of Magnevist, Dotarem, Prohance, saline, and sucrose. The results show that while the Grüneisen parameter of the saline solution does not greatly increase with concentration (<10%), the same cannot be said for the other contrast agents. This is because the concentration of the solute required to produce an increase in σ_t of the saline solution is very small; only 9 g/L of solute is required to give the maximum σ_t of the saline solutions in Fig. 6. On the other hand, the concentrations required to give the maximum σ_t of

TABLE VIII. Dielectric properties of Dotarem dilutions.

Molar conc.	ϵ_r'	$\sigma_t\|_{3\ \mathrm{GHz}}$ (S/m)	σ_c (S/m)	$\sigma_d\|_{3\ \mathrm{GHz}}$ (S/m)	$\sigma_d - \sigma_{d\mathrm{water}}$ (S/m)
0.010	78.08	2.166	0.041	2.125	0.027
0.021	77.58	2.238	0.071	2.167	0.069
0.042	76.61	2.371	0.127	2.244	0.146
0.083	74.73	2.595	0.213	2.382	0.284
0.167	71.12	2.927	0.328	2.599	0.501
0.250	67.54	3.148	0.402	2.746	0.648

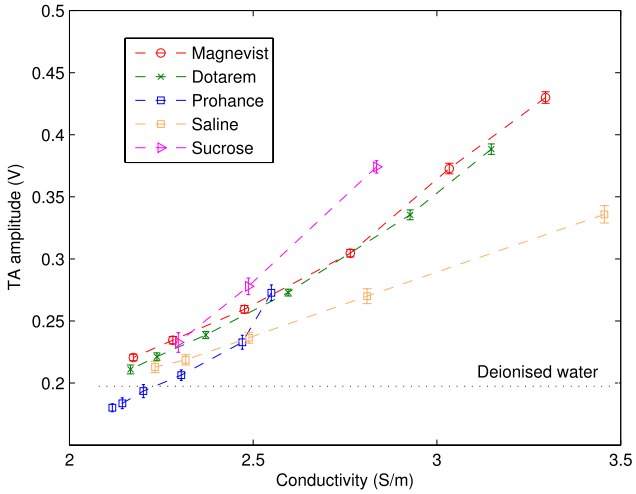

FIG. 4. Plot of measured pk–pk thermoacoustic signal amplitude against measured total conductivity for Magnevist, Dotarem and Prohance, Saline and Sucrose solutions.

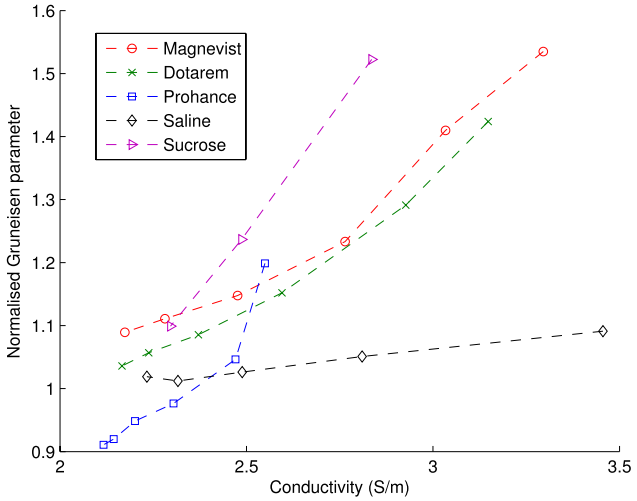

FIG. 6. Change in Grüneisen coefficient with total conductivity for different concentrations of Magnevist, Dotarem, Prohance, saline, and sucrose.

the other contrast agents in Fig. 6 are 234.5, 188.4, 139.7, and 342 g/L for Magnevist, Dotatem, Prohance, and sucrose, respectively. In order to verify the increase in Grüneisen parameter shown in Fig. 6, the expected change in the Grüneisen parameter of two sucrose solutions was calculated using values of specific heat capacity at constant pressure (C_p) and thermal volume expansivity (β) available in the literature at 20 °C,[42,43] assuming the sound speed (c) of the solutions is unchanged from that of water. The Grüneisen parameter was calculated using $\Gamma = \beta c^2/C_p$. The estimated Grüneisen parameters for the 0.5 and 1 M sucrose solution are shown in Table IX, along with values normalized to that of water (0.111). The increase in calculated values of normalized Grüneisen parameter of the sucrose solutions with concentration (1.28 and 1.69), is broadly in agreement with the increase (1.24 and 1.52) seen in Fig. 6. The implication of the data in Fig. 6 is that the measured increase in TA signal amplitude of some of the contrast agents in Fig. 4, has a very substantial contribution from the change in Grüneisen parameter. For example, the TA signal generated from a 0.25 M solution of Magnevist would be reduced by a factor of 1.5, once the increase in Grüneisen parameter is discounted.

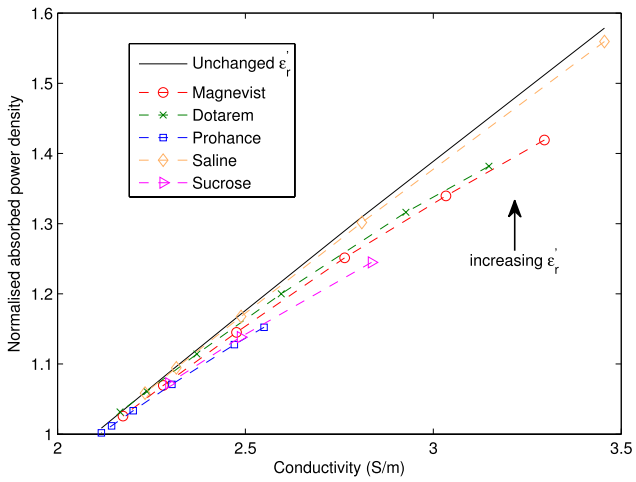

FIG. 5. Simulated changes in absorbed power density P_d (normalized to water) against total conductivity for contrast agent solutions, showing effect of change in ϵ_r'.

4. DISCUSSION

As Eq. (2) shows, the complex permittivity, ionic conductivity, complex permeability, and Grüneisen parameter all contribute to TA contrast. A clear understanding of the relative contributions of each is therefore essential for the optimal selection or design of a TA contrast agent. The following discusses the findings of this study in relation to each source of contrast and the characteristics of the three types of contrast agents investigated.

4.A. Dielectric contrast

As discussed in Sec. 1, dielectric based thermoacoustic contrast is primarily defined by the total conductivity σ_t. This in turn comprises the sum of two contributions: (i) the ionic conductivity σ_c which represents the resistive loss due to joule heating and (ii) σ_d which is associated with the frictional dielectric polarization loss due to the time-varying reorientation of polar molecules. To illustrate the dielectric contrast provided by each component individually, the dielectric properties of two reference solutions of well known dielectric behavior—saline and aqueous sucrose—were measured. Saline is a strong electrolyte containing mobile Na^+ and Cl^- ions so the contrast enhancement it provides (relative to water) is primarily due to an increase in σ_c, whereas aqueous sucrose is composed only of polar molecules and thus provides contrast based predominantly on changes in σ_d. Whether the dielectric contrast σ_t is dominated by σ_c or σ_d is largely immaterial. Indeed, Tables III and IV show that comparable values of σ_t were obtained with both solutions. However in the case of

TABLE IX. Estimated and measured thermodynamic properties of sucrose solutions.

Conc. (M)	C_P (J Kg^{-1} °C^{-1}) (Ref. 43)	β (°C^{-1}) (Ref. 42)	Γ_{sol}	Γ_{sol}/Γ_w (calculated)	Γ_{sol}/Γ_w (measured)
1.0	3585	2.99×10^{-4}	0.188	1.686	1.52
0.5	3842	2.44×10^{-4}	0.143	1.283	1.24

sucrose, this was only achieved by using very high concentrations: well over an order of magnitude higher than the saline solutions. In other words, introducing even a small number of ions into water by dissolving NaCl in water produces a very significant increase in σ_c and thus σ_t, whereas a large number of sucrose molecules are required to produce a comparable increase in σ_t via a change in σ_d. Indeed, the sucrose concentrations used in this study were so high that the Grüneisen parameter increased to the extent that it provided a significant contribution to the TA contrast (Sec. 3.B.2). For equal solute concentrations, this suggests strong electrolytes such as saline will provide much higher contrast than polar non-electrolytes at microwave frequencies. Polar molecules may still have a role to play as thermoacoustic contrast agents. This is particularly so if specific targeting is required as they are likely to be more straightforward to conjugate than electrolytic contrast agents. However to achieve adequate contrast, the excitation frequency may need to be reduced significantly so that it lies in the 10–100 s of MHz range. At these lower frequencies, σ_d contrast of solutions containing large polar molecules is typically much higher than at microwave frequencies. For example, for a 1 M glucose solution,[44] the ratio of σ_d to that of water is 1.32 at 3 GHz, increasing to 2.02 at 100 MHz and 2.53 at 10 MHz. On the other hand, increasing the excitation frequency to 6 GHz (an alternative frequency that has been used for TA imaging[12]), reduces the ratio to 1.13.

4.B. Magnetic contrast

As indicated by Eq. (3), the absorbed power density depends on the complex magnetic permeability. The latter therefore represents a potential source of TA contrast. This has led to the suggestion that contrast agents employed in MRI for their favorable magnetic properties might also provide significant magnetic based TA contrast.[16] However, as shown in Sec. 3.A.4, the absorbed power density contribution due to magnetic loss at 3 GHz is negligible, even when using MRI contrast agents that exhibit high magnetic permeability relative to water. This is because, in general, dielectric loss at microwave frequencies significantly exceeds magnetic loss which only becomes non-negligible only at much lower frequencies (kHz–MHz). For these reasons, achieving exogenous TA contrast by exploiting magnetic contrast is likely to be very challenging.

4.C. Grüneisen parameter based contrast

Contrast based on differences in the Grüneisen parameter can, in principle, be exploited to provide TA contrast. However, in practice, extremely high, potentially physiologically disruptive solute concentrations are required to provide a significant contribution. For example, a significant fraction of the TA contrast obtained using the gadolinium based contrast agents and sucrose solutions was due to the Grüneisen parameter but this required concentrations of the order of 100 g/L compared to <10 g/L for the saline solutions used in this study. The prospects for exploiting Grüneisen based exogenous contrast are therefore likely to be limited, except in circumstances where very high solute concentrations can be tolerated.

4.D. Characterization of previously reported TA contrast agents

As illustrated in Tables V, VII, and VIII, the three gadolinium based contrast agents (Magnevist, Dotarem, and Prohance) provided a modest level of dielectric contrast. However, it is important to note that this contrast was not due to the gadolinium itself. It was due either to the ionic nature of the gadolinium chelate, which dissociates from the gadolinium salt, thus increasing σ_c or the presence of the nondissociated polar fraction of the solute which increases σ_d or a combination of both. Moreover, to achieve even the limited dielectric contrast reported in this study required very high concentrations (more than an order of magnitude higher than the recommended clinical dose) to the extent that a significant component of the measured TA contrast was due to the change in the Grüneisen parameter. It therefore appears unlikely that sufficient TA contrast can be achieved using gadolinium based contrast agents at physiologically acceptable concentrations. For these reasons, there appears to be little justification for using gadolinium contrast agents in TA imaging unless perhaps as a multimodal TA-MRI contrast agent, providing that the high solute concentration required can be tolerated.

Single walled carbon nanotubes provided no measurable dielectric or TA contrast. This is not surprising as SWCNTs are both nonionic and nonpolar. However, other studies[13] have reported measurable contrast using SWCNTs. We can only speculate that this is because the SWCNTs were coated or suspended in an ionic or polar substance. The iron oxide particles that were characterized in the current study provided low but measurable dielectric contrast. The iron oxide itself provides no intrinsic contrast as it is both nonionic and nonpolar so it is most likely that the contrast was due to the polar carbodextran coating on the particles used. The absence of intrinsic contrast provided by both SWCNTs and iron oxide particles suggests both have little intrinsic merit as the base ingredient of a TA contrast agent.

5. CONCLUSION

It is concluded that, at microwave frequencies, the principal opportunities for achieving exogenous TA contrast in tissue lie in selecting contrast agents based on their dielectric properties, rather than seeking to exploit magnetic or Gruneisen parameter based contrast. Furthermore, dielectric based contrast is best achieved by the use of electrolytes to increase ionic conductivity rather than attempting to increase the dielectric polarization loss by introducing polar molecules. A number of contrast agents based on gadolinium, iron oxide, and single wall carbon nanotubes have previously been proposed as TA contrast agents. Our findings suggest that the major ingredients in these agents do not contribute to TA contrast in any way. Where appreciable contrast is observed it arises from the dielectric properties of an associated compound, the solvent or particle coating or indeed changes in the Grüneisen parameter. Furthermore, impractically high concentrations were required. As a consequence, these substances appear to have little practical advantage over simple chemical compounds such as sodium chloride which form strong electrolytes and can provide strong contrast at physiologically acceptable concentrations. It is anticipated that the results presented in this work will help inform the choice and design of contrast agents for microwave thermoacoustic imaging.

ACKNOWLEDGMENTS

The authors thank Endomagnetics UK Ltd for supplying EM1301, Craig Howes (Bracco Imaging) for supplying ProHance, Karin Schmueli (UCL Med. Phys.) for Dotarem, and Simon Walker Samuel (UCL CABI) for Magnevist, measured in this work. The authors also thank Paul Brennan (EE UCL) for the use of CST software. This work was supported by EPSRC and European union project FAMOS (FP7, ICT contract 317744).

[a]Electronic mail: o.ogunlade@ucl.ac.uk

[1]P. C. Beard, "Biomedical photoacoustic imaging," Interface Focus **1**(4), 602–631 (2011).
[2]D. M. Pozar, *Microwave Engineering* (Wiley, New York, NY, 1998).
[3]R. E. Collin, *Foundations for Microwave Engineering* (McGraw-Hill, Inc., US, 1992).
[4]The term microwave is typically used to describe electromagnetic waves with wavelengths between 1 cm and 1 m, corresponding to frequencies between 300 MHz to 30 GHz.
[5]C. Gabriel, S. Gabriel, and E. Corthout, "The dielectric properties of biological tissues: I. Literature survey," Phys. Med. Biol. **41**(11), 2231–2249 (1996).
[6]G. Ku and L. V. Wang, "Scanning microwave-induced thermoacoustic tomography: Signal, resolution, and contrast," Med. Phys. **28**(1), 4–10 (2000).
[7]R. A. Kruger *et al.*, "Thermoacoustic CT with radio waves: A medical imaging paradigm," Radiology **211**(1), 275–278 (1999).
[8]H. F Cook, "A comparison of the dielectric behaviour of pure water and human blood at microwave frequencies," Br. J. Appl. Phys. **3**(8), 249–255 (1952).
[9]M. Lazebnik *et al.*, "A large-scale study of the ultrawideband microwave dielectric properties of normal breast tissue obtained from reduction surgeries," Phys. Med. Biol. **52**(10), 2637–2656 (2007).
[10]M. Lazebnik *et al.*, "A large-scale study of the ultrawideband microwave dielectric properties of normal, benign and malignant breast tissues obtained from cancer surgeries," Phys. Med. Biol. **52**(20), 6093–6115 (2007).
[11]X. Jin, A. Keho, K. Meissner, and L. V. Wang, "Iron-oxide nanoparticles as a contrast agent in thermoacoustic tomography," Proc. SPIE **6437**, 64370E (2007).
[12]L. Nie, Z. Ou, S. Yang, and D. Xing, "Thermoacoustic molecular tomography with magnetic nanoparticle contrast agents for targeted tumor detection," Med. Phys. **37**, 4193–4200 (2010).
[13]M. Pramanik, M. Swierczewska, D. Green, B. Sitharaman, and L. V. Wang, "Single-walled carbon nanotubes as a multimodal-thermoacoustic and photoacoustic-contrast agent," J. Biomed. Opt. **14**(3), 034018 (2009).
[14]D. Byrd, G. W. Hanson, and S. K. Patch, "Carbon nanotubes for thermoacoustic contrast enhancement: Preliminary results," Proc. SPIE **7564**, 756417 (2010).
[15]X. Cai *et al.*, "Carbon nanoparticles as a multimodal thermoacoustic and photoacoustic contrast agent," Proc. SPIE **8581**, 858140 (2013).
[16]H. Qin, S. Yang, and D. Xing, "Microwave-induced thermoacoustic computed tomography with a clinical contrast agent of NMG_2[Gd (DTPA)]," Appl. Phys. Lett. **100**(3), 033701 (2012).
[17]3 GHz is a frequency commonly used for thermoacoustic imaging because high peak power pulsed sources are readily available at this frequency.
[18]U. Kaatze, "Techniques for measuring the microwave dielectric properties of materials," Metrologia **47**(2), 91–113 (2010).
[19]L. F. Chen, C. K. Ong, C. P. Neo, V. V. Varadan, and V. K. Varadan, *Microwave Electronics: Measurement and Materials Characterization* (Wiley-Blackwell, New Jersey, 2004).
[20]M. P. Robinson and J. Clegg, "Improved determination of Q-factor and resonant frequency by a quadratic curve-fitting method," IEEE Trans. Electromagn. Compat. **47**(2), 399–402 (2005).
[21]O. Ogunlade, Y. Chen, and P. Kosmas, "Measurement of the complex permittivity of microbubbles using a cavity perturbation technique for contrast enhanced ultra-wideband breast cancer detection," in *Proceedings of Engineering in Medicine and Biology Society* (IEEE, EMBC, Buenos Aires, 2010), pp. 6733–6736.
[22]U. Raveendranath and K. T. Mathew, "New cavity perturbation technique for measuring complex permeability of ferrite materials," Microwave Opt. Technol. Lett. **18**(4), 241–243 (1998).
[23]A. P. Gregory and R. N. Clarke, "A review of RF and microwave techniques for dielectric measurements on polar liquids," IEEE Trans. Dielectr. Electr. Insul. **13**(4), 727–743 (2006).
[24]R. G. Carter, "Accuracy of microwave cavity perturbation measurements," IEEE Trans. Microwave Theory Tech. **49**(5), 918–923 (2001).
[25]C. A. Balanis, *Advanced Engineering Electromagnetics* (John Wiley, New York, NY, 1989).
[26]International Commission on Non-ionizing Radiation Protection (ICNIRP), "Guidelines for limiting exposure to time-varying electric, magnetic, and electromagnetic fields (Up to 300 GHz)," Health Phys. **74**, 494–522 (1998), available at http://www.icnirp.org/cms/upload/publications/ICNIRPemfgdl.pdf.
[27]O. Ogunlade, B. Cox, and P. Beard, "Quantitative thermoacoustic image reconstruction of conductivity profiles," Proc. SPIE **8223**, 82230R (2012).
[28]O. Ogunlade and P. Beard, "Electric and magnetic properties of contrast agents for thermoacoustic imaging," Proc. SPIE **8943**, 89432V (2014).
[29]U. Kaatze, "Complex permittivity of water as a function of frequency and temperature," J. Chem. Eng. Data **34**(4), 371–374 (1989).
[30]J. B. Hasted, *Aqueous Dielectrics* (Chapman and Hall, London, 1973).
[31]P. Wang and A. Anderko, "Computation of dielectric constants of solvent mixtures and electrolyte solutions," Fluid Phase Equilib. **186**(1), 103–122 (2001).
[32]M. F. Tweedle, "The ProHance story: The making of a novel MRI contrast agent," Eur. J. Radiol. **7**(5), 225–230 (1997).
[33]C. F. Geraldes and S. Laurent, "Classification and basic properties of contrast agents for magnetic resonance imaging," Contrast Media Mol. Imaging **4**(1), 1–23 (2009).
[34]N. Wiberg, *Holleman-Wiberg's Inorganic Chemistry* (Academic, New York, NY, 2001).
[35]The conversion from molar conductivity (Λ_m in S cm^2 mmol^{-1}) to conductivity (σ_c in S cm^{-1}) is $\sigma_c = \Lambda_m \times c \times 10^{-3}$ where c is the concentration in mmol cm^3, which in this case has a value equal to 0.5.

[36]The chemical expression for Magnevist is NMG_2 (Gd-DTPA) while the compound in Ref. 32 is Na_2 (Gd-DTPA). The DC conductivities of the two solutions can be expected to be different because Magnevist dissociates as $NMG_2\,(\text{Gd-DTPA}) \longrightarrow 2NMG^{+} + (\text{Gd}-\text{DTPA})^{2-}$, while the compound in Ref. 32 dissociates as $Na_2\,(\text{Gd-DTPA}) \longrightarrow 2Na^{+} + (\text{Gd}-\text{DTPA})^{2-}$. In an MRI context (Ref. 32), both would have similar magnetic properties since they contain the same gadolinium chelate (Gd-DTPA), which is the active ingredient in MRI, hence Na_2 (Gd-DTPA) was characterised as a substitute for NMG_2 (Gd-DTPA). However, in a TA context, they are completely different compounds.

[37]J. F. Schenck, "The role of magnetic susceptibility in magnetic resonance imaging: MRI magnetic compatibility of the first and second kinds," Med. Phys. **23**, 815–850 (1996).

[38]G. Bellizzi, O. M. Bucci, and A. Capozzoli, "Broadband spectroscopy of the electromagnetic properties of aqueous ferrofluids for biomedical applications," J. Magn. Magn. Mater. **322**(20), 3004–3013 (2010).

[39]R. Hergt, S. Dutz, R. Müller, and M. Zeisberger, "Magnetic particle hyperthermia: Nanoparticle magnetism and materials development for cancer therapy," J. Phys.: Condens. Matter **18**(38), 2919–2934 (2006).

[40]Q. A. Pankhurst, N. T. Thanh, S. K. Jones, and J. Dobson, "Progress in applications of magnetic nanoparticles in biomedicine," J. Phys. D: Appl. Phys. **42**(22), 224001 (2009).

[41]J. Laufer, E. Zhang, and P. Beard, "Evaluation of absorbing chromophores used in tissue phantoms for quantitative photoacoustic spectroscopy and imaging," J. Sel. Top. Quantum Electron. **16**(3), 600–607 (2010).

[42]F. Espejo and S. Armada, "Determination of volumetric coefficients of thermal expansion in alcoholic beverages and aqueous ethanol sucrose mixtures by differential volume measurements," Food Bioprocess Technol. **5**(7), 2805–2818 (2012).

[43]M. Asadi, *Beet-Sugar Handbook* (Wiley-Blackwell, New Jersey, 2006).

[44]K. Fuchs and U. Kaatze, "Dielectric spectra of mono-and disaccharide aqueous solutions," J. Chem. Phys. **116**(16), 7137–7144 (2002).